

Energy-Efficient Synthesis and High Thermoelectric Performance of α -Cu_{2-y}Se_{1-x}Te_x

Fei-Hung Lin^[a] and Chia-Jyi Liu^{*[a]}

The high-temperature phase of β -Cu₂Se always appears as the major phase for the reaction carried out using chemical solution methods. Here, a procedure was developed that could fabricate a single phase of α -Cu₂Se_{1-x}Te_x ($x=0.02$ and 0.04) by room-temperature aqueous synthesis using NaBH₄ as reducing agent followed by cold pressing and sintering at 650 °C for 6 h in a flowing gas mixture of 20% H₂ and 80% N₂. The energy-efficient synthesis carried out at room temperature abides by the 6th principle for green chemistry with less energy

consumption. The reaction mechanism was studied, and evidence was provided of α -Cu₂Se being formed via the reaction between elemental Cu and Se atoms at room temperature. The resulting materials were characterized by powder X-ray diffraction, field-emission scanning electron microscopy, thermoelectric transport measurements, and Hall measurements. Cu_{1.96}Se_{0.96}Te_{0.04} had the highest power factor of 11 $\mu\text{Wcm}^{-1}\text{K}^{-2}$ at 818 K, and Cu₂Se_{0.96}Te_{0.04} had the maximum $zT \geq 1.4$ at $T \geq 920$ K among this series of materials.

Introduction

Thermoelectric materials can convert thermal energy to electricity. Research efforts on thermoelectrics would be beneficial in waste heat recovery. The efficiency of thermal-to-electrical (TE) energy conversion can be evaluated by the dimensionless figure of merit $zT = S^2T/\rho(\kappa_e + \kappa_l)$, where S is the thermopower (Seebeck coefficient), T the absolute temperature, ρ the electrical resistivity, κ_e the electronic thermal conductivity, and κ_l the lattice thermal conductivity, respectively. Therefore, materials with high zT values require low electrical resistivity, large thermopower, and low thermal conductivity. Generally, the strategies of enhancing TE performance include band engineering, nanostructuring, compositing, fabricating various-scale hierarchical architecture, and others.

Cu₂Se, one of copper chalcogenides, has a simple chemical formula but complex atomic arrangements. Copper selenide has been intensively investigated in a number of fields of research such as thermoelectrics,^[1–8] batteries,^[9,10] solar cells,^[11–13] optics,^[14–18] electrochemistry,^[19,20] and thermal physics.^[21] It is well known that Cu₂Se undergoes structural phase transition from monoclinic (α -phase) to face-centered cubic at about 413 K. Hydrothermally^[7,22–25] or solvothermally^[8,26,27] synthesized Cu₂Se always results in a high-temperature phase (β -Cu₂Se). Moreover, some groups report methods that are able to facilitate the transformation of β -phase to α -phase by Te doping or adding SbCl₃ in the reaction but could not produce single phase of low-temperature structure (α -phase).^[8,26] It would be therefore interesting to grow a single phase of α -Cu₂Se at room temperature using solution-based chemical methods based on the following objectives: (1) to clarify why β -

Cu₂Se is always obtained using solution methods instead of the pure α -Cu₂Se phase being directly synthesized using melting process; (2) to obtain intrinsic transport and optical properties of α -Cu₂Se synthesized using solution methods since Cu₂Se synthesized by sputtering^[12] and thermal evaporation^[13] in solar cell studies is also the β -phase. Due to the low electrical resistivity, large thermopower, and low thermal conductivity, Cu₂Se is one of the potential thermoelectric materials. Among the recent reports, Cu₂Se exhibits a zT of about 1.4–1.8 at around 800–1000 K.^[1–8]

For human sustainable development, both issues of energy and environment protection need to be tackled in pursuing economic growth. In the 6th principle of “Design for Energy Efficiency” for green chemistry,^[28] chemical processes are suggested to be conducted at ambient temperature and pressure for minimizing the energy requirement on environmental and economic impacts. We have aimed to follow this guideline for energy consumption in fabricating thermoelectric materials.^[29,30] In this work, we report the synthesis and thermoelectric property measurements of a series of Cu_{2-y}Se_{1-x}Te_x with $(x,y) = (0.02, 0)$, $(0.04, 0)$, $(0.04, 0.02)$, and $(0.04, 0.04)$ using an aqueous solution method carried out at room temperature followed by consolidation in a flowing gas mixture of 20% H₂ and 80% N₂ at 650 °C for 6 h and then under vacuum at 650 °C for another 6 h. The formation mechanism of α - and β -Cu₂Se is studied in detail, and the transformation of β -Cu₂Se to α -Cu₂Se is made possible using reductive heat treatment in an atmosphere of 20% H₂ and 80% N₂. Among this series of materials, a $zT = 1.4$ is attained at 920 K for Cu₂Se_{0.96}Te_{0.04}.

[a] Dr. F.-H. Lin, Prof. C.-J. Liu
Department of Physics
National Changhua University of Education
No.1, Jinde Rd., Changhua City, Changhua County 50007, (Taiwan)
E-mail: liucj@cc.ncue.edu.tw

Results and Discussion

Effects of washing procedure on the transformation between α -Cu₂Se and β -Cu₂Se

The low-temperature phase of α -Cu₂Se can be easily obtained by melting processes.^[1,3] However, the high-temperature phase of β -Cu₂Se persistently appears as the major phase with the presence of α -phase as minor phase in wet-chemical synthesis using hydrothermal or solvothermal methods.^[5,7,8,22,25,27] This situation is distinctly different from that in melting process. In the effort to synthesize pure α -phase, we discover that pure α -phase exists only in the as-synthesized powders without the presence of β -phase when the powders are taken out of the reaction beakers without further washing. Since in the wet-chemical synthesis, de-ionized (DI) water and ethanol are often adopted to wash away remaining chemicals in the routine practice, we reckon that the washing procedure might be associated with the transformation of α -phase to β -phase. As shown in the X-ray diffraction (XRD) patterns of Figure 1, α -Cu₂Se only exists in the as-synthesized powers without going through washing procedure; part of α -Cu₂Se transforms to β -Cu₂Se, which becomes the major phase co-existing with relatively large amount of Cu₂O after washing with DI water. This result suggests that mobile Cu ions on the un-passivated surface sites of Cu₂Se nanoparticles are highly reactive and react with surrounding oxygen to form Cu₂O. However, in the case of washing using ethanol instead of DI water, there is no sign of Cu₂O formation but only a mixture of α - and β -Cu₂Se, which suggests that Cu ions are not capable of grabbing oxygen atoms to form Cu₂O from the ethanol environment.

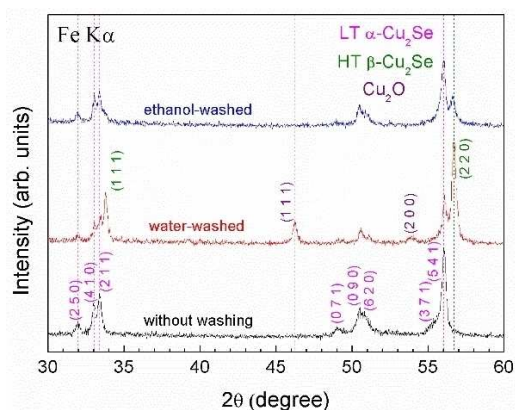


Figure 1. XRD patterns of as-synthesized Cu₂Se powders taken out of the solution after reaction at room temperature without washing, powders washed with de-ionized water, and powders washed with ethanol. LT α -Cu₂Se: low-temperature phase with Miller indices labelled in pink; HT β -Cu₂Se: high temperature phase with Miller indices labelled in green; Cu₂O with Miller indices labelled in black. Vertical lines are a guide for the eye.

Proposed reaction mechanism of aqueous synthesis of α -Cu₂Se at room temperature

In order to better understand the formation mechanism of α -Cu₂Se synthesized at room temperature, several experiments were carried out. CuCl₂·2H₂O was first dissolved in DI water followed by slow addition of NaBH₄. Upon addition of NaBH₄, Cu²⁺ ions are reduced by BH₄⁻ to Cu nanoparticles (Cu NPs) with evolution of H₂ gas bubbling in the flask. As shown in Figure 2, the broad XRD peaks indicate the small sizes of Cu NPs in the form of black aggregates with the presence of Cu₂O. The formation of Cu₂O arises from the reaction between Cu NPs and oxygen in the air during taking photos shown in Figure 5. Element Se is added to the aqueous solution containing Cu NPs aggregates and becomes polyselenides, Se_x²⁻, via the reductive reaction between Se and BH₄⁻. Consequently, Cu NPs reacts quickly with the active Se released from polyselenides to form α -Cu₂Se in 5 min.

Figure 3 shows the XRD patterns for the resulting powders for the reaction duration of 5 min and overnight. It can be

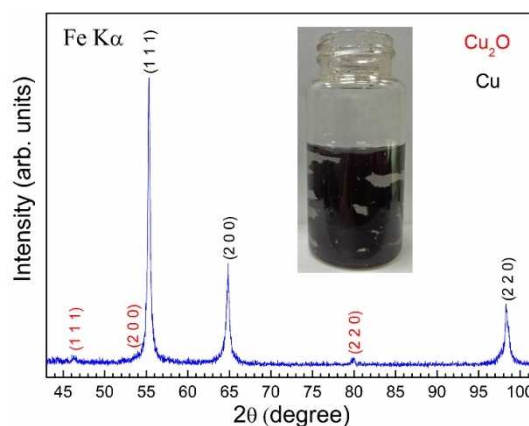


Figure 2. XRD pattern of Cu NPs. The broad XRD peaks indicate small sizes of Cu NPs coexisting with Cu₂O. The formation of Cu₂O arises from the reaction between Cu NPs and oxygen in the air while taking photos shown in Figure 5. The inset shows the Cu NPs aggregating in the aqueous solution.

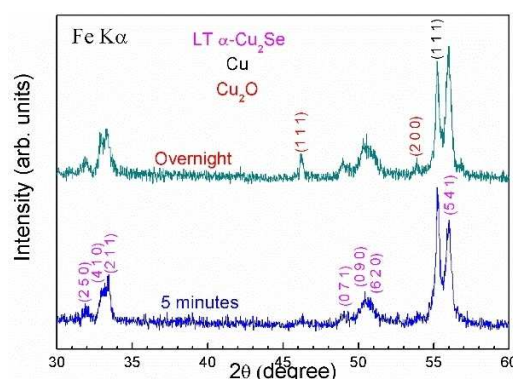
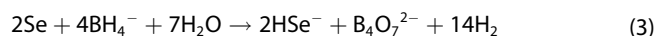
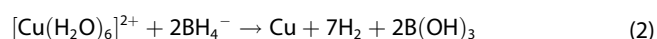
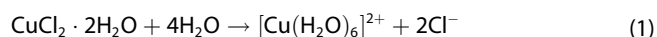


Figure 3. XRD patterns of α -Cu₂Se synthesized by adding Se element into the solution containing Cu NPs for the reaction duration of (a) 5 min and (b) overnight. The α -Cu₂Se forms immediately by the reaction between active Se and Cu NPs.

readily seen that α -Cu₂Se forms in 5 min as the Se is added into the solution containing Cu NPs aggregates. Moreover, as the above solution sits still overnight, both the α -Cu₂Se (541) and Cu₂O (111) peaks grow as compared to the Cu (111) peak, indicating some of the Cu NPs aggregates gradually transforms to α -Cu₂Se, part of which releases some Cu from the lattice to react with surrounding oxygen and form Cu₂O. Accordingly, the formation mechanism of α -Cu₂Se is proposed as follows [Eqs. (1)–(6)]:



As shown in the first vial from the left in Figure 4a, as CuCl₂·2H₂O is dissolved in DI water, the aqueous solution becomes [Cu(H₂O)₆]²⁺ complex with blue color as described in Equation (1). As NaBH₄ is slowly added to the aqueous solution, the [Cu(H₂O)₆]²⁺ complex is reduced by BH₄⁻ to Cu NPs,^[31] shown in the second vial from the left in Figure 4a, with evolution of H₂ gas, which then form aggregates settling down at the bottom of the vial as shown in the third vial from the left in Figure 4a and Equation (2). As the Se element is added to the solution containing Cu NPs aggregates, α -Cu₂Se forms immediately with the red color appearing on the top portion of the vial, which can be seen in the fourth vial from the left in Figure 4a.

As described in Equations (3) and (4),^[32] the Se element is first reduced by BH₄⁻ to HSe⁻, which is then oxidized by the oxygen from the air to Se₂²⁻. Generally speaking, polyselenides Se_x²⁻ only exists in a very basic solution.^[33] In our reaction, no alkali is added; nevertheless the pale red color of Se₂²⁻ appears

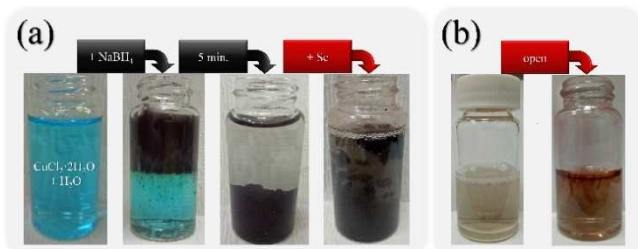


Figure 4. (a) Photos showing the process of atom-atom reaction. The CuCl₂·2H₂O is first dissolved in DI water. The Cu NPs form upon the addition of NaBH₄. After blue color disappears, the Se element powders are added to the solution containing Cu NP aggregates, and α -Cu₂Se forms immediately with red color appearing in the solution before the reaction completes. (b) Photos showing the formation of red Se₂²⁻ upon opening the cap of the vial, which has the aqueous solution containing Se powders and NaBH₄.

on the top portion of the vial.^[34] Since the pale red color is not clear enough in the photo to show the presence of Se₂²⁻, Figure 4b illustrates that the clear aqueous solution containing Se element and NaBH₄ turns into red Se₂²⁻ on the top surface of the solution as the cap of the vial is opened to allow the top surface of aqueous solution to be in contact with air. It should be noted that the red color disappears after the cap is closed and made airtight and the solution is shaken. As described in Equations (5) and (6), active Se released from Se₂²⁻ reacts with Cu NPs aggregates to form α -Cu₂Se. To further illustrate that the reaction occurs between Cu atoms and Se atoms, Cu NPs are pressed into a bar and then put into a polyselenides solution.

Figure 5a is the rectangle bar made of Cu NPs showing a metal luster of copper. Figure 5b shows that the metallic luster surface turns into dull black upon immersing the Cu bar in the solution containing Se element and NaBH₄. This indicates that red copper transforms into α -Cu₂Se on the surface of the copper bar. Upon polishing the left part of the bar, Figure 5c shows that the metallic luster of copper appears again on the surface.

XRD and microstructure of sintered α -Cu_{2-y}Se_{1-x}Te_x

Even with the knowledge that part of α -Cu₂Se transforms into β -Cu₂Se after the washing procedure, washing away Na⁺, BH₄⁻, and Cl⁻ is necessary to avoid unnecessary disturbance in transport measurements. To avoid oxidation,^[35] the washed and dried powders were cold-pressed and sintered at 650 °C for 6 h in a reducing atmosphere environment. Figure 6 shows the XRD patterns of Cu_{2-y}Se_{1-x}Te_x with (x, y) = (0.02, 0), (0.04, 0), (0.04, 0.02), and (0.04, 0.04) synthesized using the aqueous solution method at room temperature followed by sintering at 650 °C for 6 h in a flowing gas mixture of 20% H₂ and 80% N₂. Samples without Cu deficiency (y = 0) are of single-phase α -Cu₂Se.

This is distinctly different from those Cu₂Se mixtures consisting of α - and β -phase synthesized using hydrothermal or solvothermal reaction. The XRD peaks shift to lower 2 θ as the Te content increases, indicating that the lattice expansion arises from the larger ionic radius of Te²⁻. The lattice parameters for samples with different Te contents are refined and shown in Table 1. These results indicate that lattice expansion occurs with partial replacement of Te on the Se sites in the lattice. However, samples with Cu deficiency (y \neq 0) are a mixture of α - and β -Cu₂Se. Based on these results, it seems that the starting

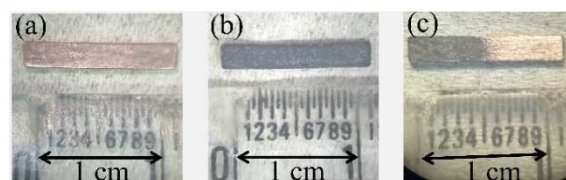


Figure 5. Photos showing (a) the red Cu bar made by cold-pressing Cu NPs; (b) dull black α -Cu₂Se forms on the surface of the Cu bar; (c) partially polishing away α -Cu₂Se and exposing the red Cu.

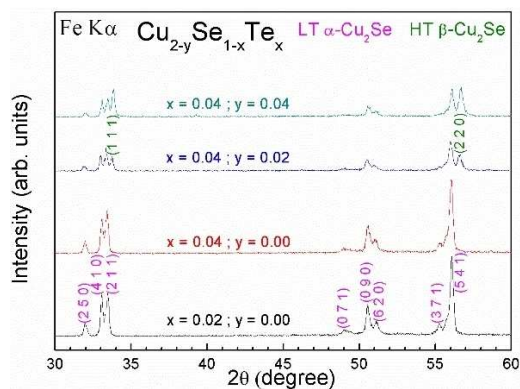


Figure 6. XRD patterns of room-temperature synthesized $\text{Cu}_{2-y}\text{Se}_{1-x}\text{Te}_x$ with $(x, y) = (0.02, 0)$, $(0.04, 0)$, $(0.04, 0.02)$, and $(0.04, 0.04)$ followed by sintering at 650°C for 6 h in a flowing gas mixture of 20% H_2 and 80% N_2 .

Material	Lattice parameters			
	a [Å]	b [Å]	c [Å]	β [°]
$x=0.02; y=0$	7.135(1)	12.368(2)	27.315(2)	94.29(1)
$x=0.04; y=0$	7.137(1)	12.376(1)	27.309(1)	94.42(1)

composition with Cu deficiency favors formation of a mixed phase and is in favor of $\beta\text{-Cu}_2\text{Se}$ as Cu deficiency increases, which is evidenced by the peak intensity of the (111) reflection from $\beta\text{-Cu}_2\text{Se}$.

Figure 7 shows the field-emission scanning electron microscopy (FE-SEM) images of $\text{Cu}_{2-y}\text{Se}_{1-x}\text{Te}_x$ with $(x, y) = (0.02, 0)$, $(0.04, 0)$, $(0.04, 0.02)$, and $(0.04, 0.04)$. These images exhibit morphologies consisting of varied-size plates, chunks, lumps, and small particles. Moreover, the number of small particles adhered to the chunks increases with the doping content of Te,

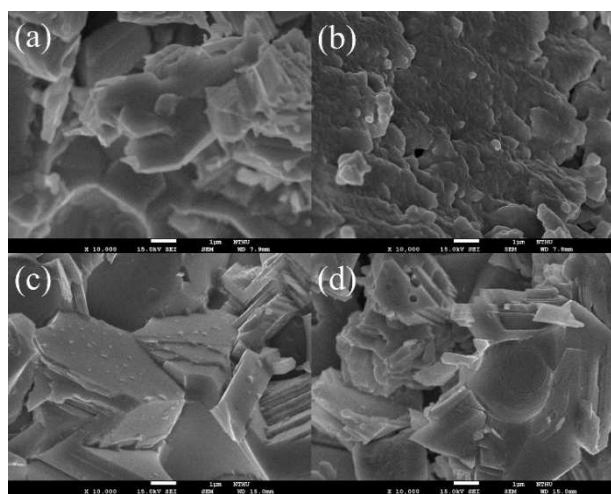


Figure 7. FE-SEM images of as-sintered $\text{Cu}_{2-y}\text{Se}_{1-x}\text{Te}_x$ with (a) $(x, y) = (0.02, 0)$; (b) $(x, y) = (0.04, 0)$; (c) $(x, y) = (0.04, 0.02)$; (d) $(x, y) = (0.04, 0.04)$. The size of scale bars is 1 μm .

which might be caused by the lattice mismatch introduced by Te dopants.

Temperature-dependent thermoelectric properties of $\text{Cu}_{2-y}\text{Se}_{1-x}\text{Te}_x$

Figure 8 shows the electronic transport of $\text{Cu}_{2-y}\text{Se}_{1-x}\text{Te}_x$ with $(x, y) = (0.02, 0)$, $(0.04, 0)$, $(0.04, 0.02)$, and $(0.04, 0.04)$. It can be readily seen that introducing Cu deficiency significantly reduces both the electrical resistivity and thermopower due to enhanced hole carriers by introducing Cu defects. This is consistent with the increased Hall carrier concentration in Cu-deficient samples as shown in Figure 9. Moreover, both the electrical resistivity and thermopower exhibit metal-like temperature dependence. The power factor exhibits a broad maximum due to a more rapid increase of electrical resistivity than thermopower above 700 K. The highest power factor of $11 \mu\text{W cm}^{-1} \text{K}^{-2}$ at 818 K is attained for the $(x, y) = (0.04, 0.04)$ sample.

The total thermal conductivity (κ) of a solid consists of contributions of the charge carriers and the lattice vibrations, namely, $\kappa = \kappa_e + \kappa_l$, where κ_e and κ_l represent the electronic and lattice thermal conductivity, respectively. As seen in Figure 8d, the phase-transition temperature seen in κ of $\text{Cu}_{2-y}\text{Se}_{1-x}\text{Te}_x$ is consistent with that measured in electrical resistivity. Since the double spiral sensor used in the Hot Disk (TPS 2500S) is made of Ni, which has a Curie temperature of 627 K, we did not carry out the measurements at $573 < T < 700$ K. Moreover, since κ tends to decrease with increasing temperature, we take the data of $\kappa_{T_{\text{max}}}$ for $T \geq T_{\text{max}}$, where $\kappa_{T_{\text{max}}}$ is the total thermal conductivity measured at the maximum temperature T_{max} we carry out in the experiments, in consideration of the costly Hot Disk sensor, which easily deteriorates after a few thermal cycles going through high temperatures. All the κ falls in the range of 1.0 and 2.1 below 600 K, and within the range of 0.6 to 1.9 above 700 K. In order to see the extent of electronic contribution to κ , we estimate κ_e from the electrical conductivity using the Wiedemann–Franz law given by Equation (7):

$$\frac{\kappa_e}{\sigma} = \frac{\pi^2}{3} \left(\frac{k_B}{e} \right)^2 T = L_0 T \quad (7)$$

where k_B is the Boltzmann constant, σ is the electrical conductivity, and L_0 is the Lorenz number calculated using an algorithm called SPBcal within the framework of single parabolic band (SPB) model under an acoustic phonon scattering assumption [Eq. (8)]:^[36–39]

$$L = \left(\frac{k_B}{e} \right)^2 \left[\frac{3F_2(\eta)}{F_0(\eta)} - \left(\frac{2F_2(\eta)}{F_0(\eta)} \right)^2 \right] \quad (8)$$

where $F_0(\eta)$ and $F_2(\eta)$ are, respectively, the index $n=0$ and 2 of the Fermi–Dirac integrals given by Equation (9):

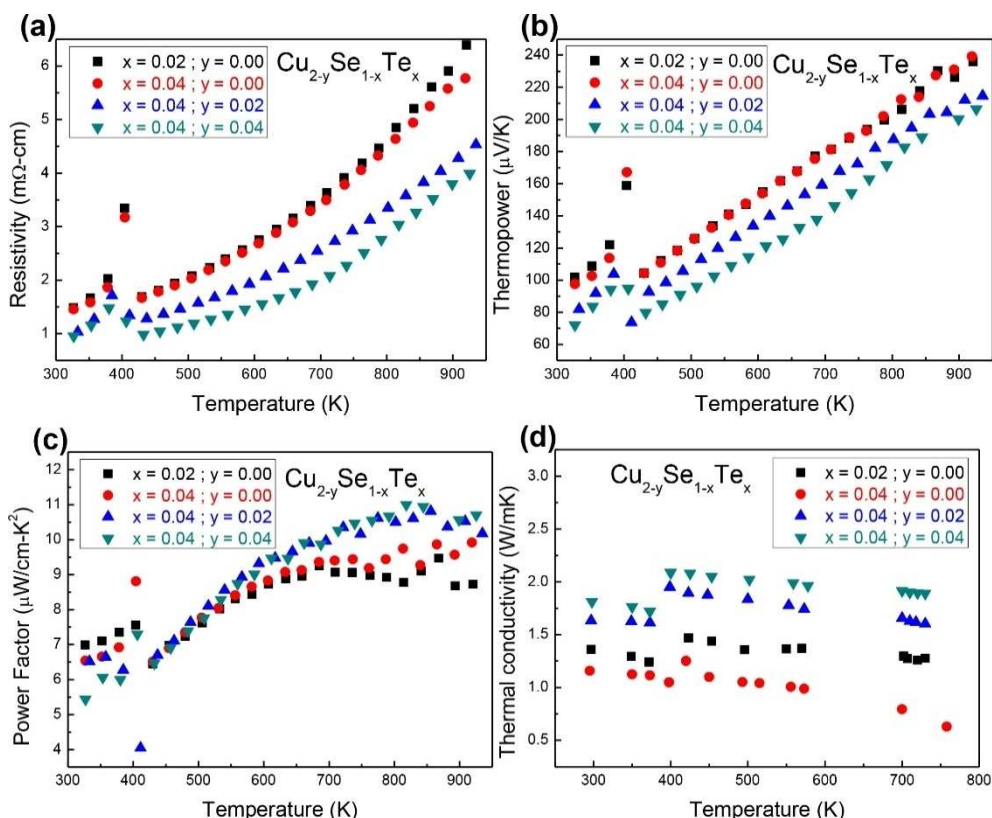


Figure 8. Temperature dependence of (a) resistivity; (b) thermopower; (c) power factor; and (d) thermal conductivity for room-temperature synthesized $\text{Cu}_{2-y}\text{Se}_{1-x}\text{Te}_x$ with $(x, y) = (0.02, 0)$, $(0.04, 0)$, $(0.04, 0.02)$, and $(0.04, 0.04)$ followed by sintering at 650°C for 6 h in a flowing gas mixture of 20% H_2 and 80% N_2 and then under vacuum for another 6 h.

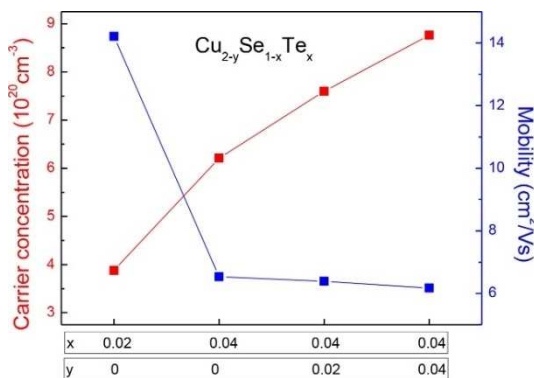


Figure 9. Room-temperature Hall carrier concentration and mobility for room-temperature synthesized $\text{Cu}_{2-y}\text{Se}_{1-x}\text{Te}_x$ with $(x, y) = (0.02, 0)$, $(0.04, 0)$, $(0.04, 0.02)$, and $(0.04, 0.04)$ followed by sintering at 650°C for 6 h in a flowing gas mixture of 20% H_2 and 80% N_2 and then under vacuum for another 6 h.

$$F_n(\eta) = \int_0^\infty \frac{x^n}{1 + \exp(x - \eta)} dx. \quad (9)$$

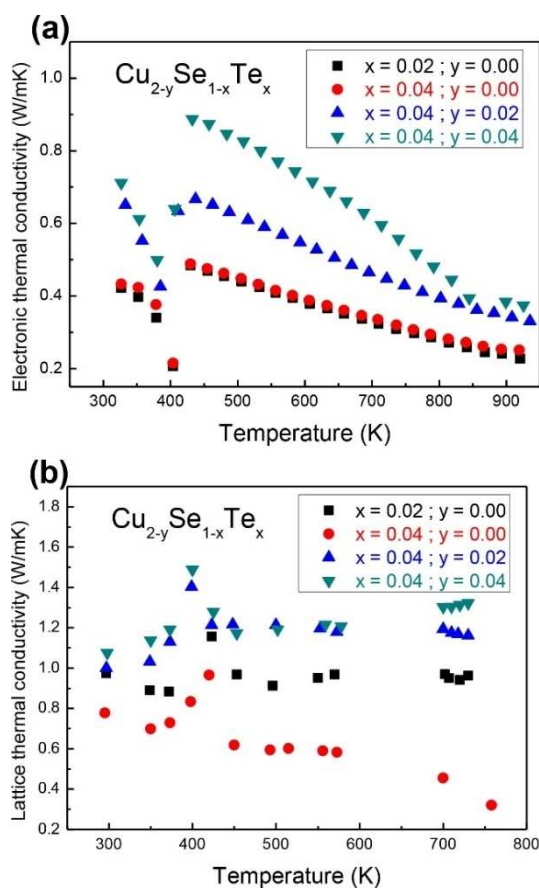
The calculated transport parameters of $\text{Cu}_{2-y}\text{Se}_{1-x}\text{Te}_x$ with $(x, y) = (0.02, 0)$, $(0.04, 0)$, $(0.04, 0.02)$, and $(0.04, 0.04)$ are listed in Table 2.

Figure 10 shows the temperature dependence of calculated κ_e and κ_l based on the Wiedemann–Franz law. As seen in Figure 10a, the charge carriers play a significant role in the contribution to κ , which is expected for materials with high electrical conductivity. It is noted that electronic contribution to κ is 40–50% above the phase-transition temperature at $T > 450$ K for the sample with $(x, y) = (0.04, 0)$. Moreover, the κ_l of $\text{Cu}_{2-y}\text{Se}_{1-x}\text{Te}_x$ with $x = 0.04$ increases with increasing y (Cu deficiency) at $T \geq 550$ K. The Cu content determined from inductively coupled plasma mass spectrometry (ICP-MS; Table 3) might shed some light on the increasing trend of κ_l with increasing Cu deficiency (y) in $\text{Cu}_{2-y}\text{Se}_{1-x}\text{Te}_x$ with $x = 0.04$. Since the disordered copper ions are superionic with liquid-like mobility around the rigid Se face-centered cubic lattice of Se, this leads to a considerably low lattice thermal conductivity. This scenario might be responsible for larger κ_l in $\text{Cu}_{2-y}\text{Se}_{1-x}\text{Te}_x$ with $x = 0.04$ with fewer superionic Cu ions in the lattice acting like liquid and creating less disorder to disrupt thermal transport of phonons.^[1] As seen in Table 2, the Cu content in the $y = 0$ sample has more Cu ions than others in $\text{Cu}_{2-y}\text{Se}_{1-x}\text{Te}_x$ with $x = 0.04$ and hence has the smallest κ_l .

Figure 11 shows the temperature dependence of zT for $\text{Cu}_{2-y}\text{Se}_{1-x}\text{Te}_x$ with $(x, y) = (0.02, 0)$, $(0.04, 0)$, $(0.04, 0.02)$, and $(0.04, 0.04)$ synthesized using aqueous solution method at room temperature followed by sintering at 650°C for 6 h in a flowing gas mixture of 20% H_2 and 80% N_2 and then under vacuum for

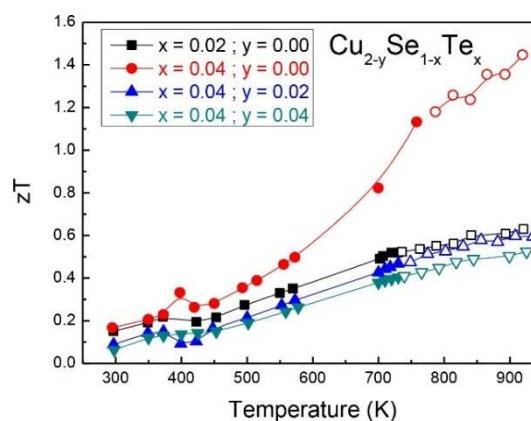
Table 2. Room-temperature transport parameters calculated SPB model for $\text{Cu}_{2-y}\text{Se}_{1-x}\text{Te}_x$ with $(x, y) = (0.02, 0), (0.04, 0), (0.04, 0.02),$ and $(0.04, 0.04)$. The free electron mass (m_0) is 9.11×10^{-31} kg.

Parameters	$x=0.02$ $y=0$	$x=0.04$ $y=0$	$x=0.04$ $y=0.02$	$x=0.04$ $y=0.04$
Thermopower [$\mu\text{V K}^{-1}$]	101.0	99.01	69.45	58.21
Hall mobility [$\text{cm}^2 \text{V}^{-1} \text{s}^{-1}$]	14.20	6.532	6.387	6.170
Hall concentration [10^{20}cm^{-3}]	3.877	6.208	7.597	8.762
Reduced Fermi energy	2.4	2.5	3.9	4.8
Effective mass [$m^* m_0^{-1}$]	2.87	3.83	2.94	2.66
κ_{total} [W mK^{-1}]	1.36	1.16	1.63	1.81
κ_e [W mK^{-1}]	0.385	0.379	0.633	0.737
κ_l [W mK^{-1}]	0.974	0.778	1.00	1.08
Hall factor R_H	1.067	1.065	1.040	1.030
Carrier concentration [10^{20}cm^{-3}]	4.136	6.610	7.899	9.022
Carrier mobility [$\text{cm}^2 \text{V}^{-1} \text{s}^{-1}$]	24.50	11.41	13.13	13.84
Quality factor	18589	16419	10072	8572.7

**Figure 10.** Temperature dependence of (a) electronic (κ_e) and (b) lattice thermal conductivity (κ_l) for room-temperature synthesized $\text{Cu}_{2-y}\text{Se}_{1-x}\text{Te}_x$ with $(x, y) = (0.02, 0), (0.04, 0), (0.04, 0.02),$ and $(0.04, 0.04)$ followed by sintering at 650°C for 6 h in a flowing mixture gas of 20% H_2 and 80% N_2 and then under vacuum for another 6 h.

another 6 h. A $zT = 1.4$ is attained at 920 K for the $(x, y) = (0.04, 0)$ sample. The high zT value arises mainly from its low κ_e and κ_l among this series of materials. In view of the decreasing trend of κ with increasing temperature in this work and data reported in the literature, the zT value is expected to be higher than 1.4.

Table 4 compares the Cu_2Se fabricated by a combination of melting process and spark plasma sintering with our fabrication

**Figure 11.** Temperature dependence of zT for room-temperature synthesized $\text{Cu}_{2-y}\text{Se}_{1-x}\text{Te}_x$ with $(x, y) = (0.02, 0), (0.04, 0), (0.04, 0.02),$ and $(0.04, 0.04)$ followed by sintering at 650°C for 6 h in a flowing gas mixture of 20% H_2 and 80% N_2 and then under vacuum for another 6 h. The open symbols are the magnitude of calculated zT for $T \geq T_{\kappa, \text{max}}$ where $T_{\kappa, \text{max}}$ is the maximum temperature in our thermal conductivity measurements. Note that the total thermal conductivity tends to decrease with increasing temperature in this system.

method involving room-temperature aqueous synthesis followed by heating at 650°C for 6 h under a flowing gas mixture of 20% H_2 and 80% N_2 and then in vacuum at 650°C for 6 h. It can be readily seen that our fabrication procedure is an energy-efficient method.

Conclusion

A series of $\text{Cu}_{2-y}\text{Se}_{1-x}\text{Te}_x$ with $(x, y) = (0.02, 0), (0.04, 0), (0.04, 0.02),$ and $(0.04, 0.04)$ was synthesized by aqueous solution method using NaBH_4 as reducing agent at room temperature. We proposed the reaction mechanism for the formation of α - Cu_2Se . We also provided the evidence of α - Cu_2Se being formed via the reaction between elemental Cu and Se atoms at room temperature. A portion of the low-temperature phase of α - $\text{Cu}_2\text{Se}_{1-x}\text{Te}_x$ spontaneously transformed to the high-temperature phase of β - $\text{Cu}_2\text{Se}_{1-x}\text{Te}_x$ during the washing procedure. We developed a procedure to fabricate single phase of α -

Table 3. ICP-MS analyses of $\text{Cu}_{2-y}\text{Se}_{1-x}\text{Te}_x$ with $(x, y) = (0.04, 0), (0.04, 0.02),$ and $(0.04, 0.04)$. The chemical formula is calculated by setting the total amount of Se and Te as 1.

Composition (x, y)	Cu [at%]	Se [at%]	Te [at%]	Formula
(0.04, 0)	66.48	32.24	1.280	$\text{Cu}_{1.983}\text{Se}_{0.962}\text{Te}_{0.038}$
(0.04, 0.02)	66.39	32.39	1.218	$\text{Cu}_{1.975}\text{Se}_{0.964}\text{Te}_{0.036}$
(0.04, 0.04)	66.07	32.71	1.222	$\text{Cu}_{1.947}\text{Se}_{0.964}\text{Te}_{0.036}$

Table 4. Comparison of fabrication methods of Cu_2Se between published reports and our method in this study, which appears to be energy efficient as compared to others. SPS is an abbreviation for a sintering technique of spark plasma sintering.

Method	Synthesis	Consolidation	Ref.
melting process + SPS	1423 K for 12 h and 1073 K in 24 h and held for 7 days	SPS at 710 K under 65 MPa	[1]
melting process + SPS	1403 K for 10 h and 1173 K for 10 h followed by quenching in liquid nitrogen	SPS at 923 K for 5 min under 50 MPa	[3]
aqueous synthesis + pressureless sintering	room temperature	heating at 650 °C for 6 h in a flowing gas mixture of 20% H_2 and 80% N_2 followed by in vacuum at 650 °C for 6 h.	this study

$\text{Cu}_2\text{Se}_{1-x}\text{Te}_x$ ($x = 0.02$ and 0.04) by cold-pressing the washed and dried mixtures followed by sintering at 650 °C for 6 h in a flowing gas mixture of 20% H_2 and 80% N_2 . As such a single phase of $\alpha\text{-Cu}_2\text{Se}_{1-x}\text{Te}_x$ was fabricated for the first time using powders synthesized by chemical solution-based methods. However, a mixture of phases of $\alpha\text{-}$ and $\beta\text{-Cu}_{2-y}\text{Se}_{0.96}\text{Te}_{0.04}$ ($y = 0.02$ and 0.04) could only be fabricated for Cu-deficient samples. Among this series of materials, $\text{Cu}_{1.96}\text{Se}_{0.96}\text{Te}_{0.04}$ has the highest power factor of $11 \mu\text{W cm}^{-1} \text{K}^{-2}$ at 818 K, and $\text{Cu}_2\text{Se}_{0.96}\text{Te}_{0.04}$ has the highest $zT \geq 1.4$ at 920 K.

Experimental Section

Aqueous synthesis of $\text{Cu}_{2-y}\text{Se}_{1-x}\text{Te}_x$ at room temperature

A series of $\text{Cu}_{2-y}\text{Se}_{1-x}\text{Te}_x$ with $(x, y) = (0.02, 0), (0.04, 0), (0.04, 0.02),$ and $(0.04, 0.04)$ was synthesized using aqueous solution method at room temperature. $\text{CuCl}_2 \cdot 2\text{H}_2\text{O}$ was dissolved in DI water with stirring, followed by addition of Se and Te. NaBH_4 was then added slowly to the above solution. The redox reaction proceeded vigorously accompanied by formation of many bubbles. The precipitated powders were filtered and washed by DI water several times and dried in a vacuum oven at 80 °C for 5 h. For thermoelectric property measurements, the dried powders were cold-pressed into cylindrical specimens, followed by sintering at 650 °C for 6 h in a tube furnace with a flowing gas mixture of 20% H_2 and 80% N_2 . To facilitate the electronic and thermal transport measurements, the resulting bulks were reground and then re-pressed followed by sintering in a vacuum furnace at 650 °C for another 6 h. The electronic and thermal transport properties were characterized on the parallelepiped bulks cut from the same cylindrical disk.

Characterization

The phase identification was carried out using a Shimadzu XRD-6000 diffractometer. The microstructural images were taken by a JEOL JSM-7610F FE-SEM. The chemical composition of the materials was determined using Agilent 7500ce ICP-MS. The electrical resistivity and thermopower measurements were carried out using a Setaram SeebeckPro system. The thermal conductivity was measured using a Hot Disk thermal constants analyzer (TPS 2500S).

The Hall carrier concentration and mobility at room temperature were determined using the van der Pauw method equipped with a Keithley 2430 C constant current source and a Keithley 2182 A nanovoltmeter under a magnetic field of 0.6 T. The uncertainty for the electrical resistivity, thermopower, and thermal conductivity is about $\pm 10, \pm 7,$ and $\pm 5\%$, respectively.

Acknowledgements

This work was supported by Ministry of Science and Technology of Taiwan under the Grant No. 107-2112-M-018-006-MY3.

Conflict of Interest

The authors declare no conflict of interest.

Keywords: inorganic chemistry · nanostructuring · room-temperature synthesis · Te-doped Cu_2Se · thermoelectrics

- [1] H. Liu, X. Shi, F. Xu, L. Zhang, W. Zhang, L. Chen, Q. Li, C. Uher, T. Day, G. J. Snyder, *Nat. Mater.* **2012**, *11*, 422–425.
- [2] F. S. Liu, Z. N. Gong, M. J. Huang, W. Q. Ao, Y. Li, J. Q. Li, *J. Alloys Compd.* **2016**, *688*, 521–526.
- [3] F. S. Liu, M. J. Huang, Z. N. Gong, W. Q. Ao, Y. Li, J. Q. Li, *J. Alloys Compd.* **2015**, *651*, 648–654.
- [4] B. Yu, W. Liu, S. Chen, H. Wang, H. Wang, G. Chen, Z. Ren, *Nano Energy* **2012**, *1*, 472–478.
- [5] L. Yang, Z. Chen, G. Han, M. Hong, Y. Zou, J. Zou, *Nano Energy* **2015**, *16*, 367–374.
- [6] P. Peng, Z. N. Gong, F. S. Liu, M. J. Huang, W. Q. Ao, Y. Li, J. Q. Li, *Intermetallics* **2016**, *75*, 72–78.
- [7] A. Bhaskar, C.-H. Hu, C.-L. Chang, C.-J. Liu, *J. Eur. Ceram. Soc.* **2016**, *36*, 2755–2760.
- [8] L. Yang, Z.-G. Chen, G. Han, M. Hong, L. Huang, J. Zou, *J. Mater. Chem. A* **2016**, *4*, 9213–9219.
- [9] F. Rong, Y. Bai, T. Chen, W. Zheng, *Mater. Res. Bull.* **2012**, *47*, 92–95.
- [10] G. Mattsson, L. Nyholm, Å. Olin, *J. Electroanal. Chem.* **1994**, *379*, 49–61.
- [11] S. C. Park, D. Y. Lee, B. T. Ahn, K. H. Yoon, J. Song, *Sol. Energy Mater. Sol. Cells* **2001**, *69*, 99–105.
- [12] C. H. Jeong, J. H. Kim, *Thin Solid Films* **2014**, *550*, 660–664.
- [13] A. Mohan, S. Rajesh, *Superlattices Microstruct.* **2015**, *85*, 638–645.

- [14] S. Kashida, W. Shimosaka, M. Mori, D. Yoshimura, *J. Phys. Chem. Solids* **2003**, *64*, 2357–2363.
- [15] A. Mohan, S. Rajesh, G. Srikes, *Superlattices Microstruct.* **2016**, *93*, 261–268.
- [16] B. Anand, M. Molli, S. Aditha, T. M. Rattan, S. Sankara, S. Sai, V. Kamiseti, *Opt. Commun.* **2013**, *304*, 75–79.
- [17] F. Gao, L. Zhu, Y. Wang, H. Xie, J. Li, *Mater. Lett.* **2016**, *183*, 425–428.
- [18] S. Govindraj, M. P. Kalenga, M. Airo, M. J. Moloto, L. M. Sikhwivhilu, N. Moloto, *Opt. Mater.* **2014**, *38*, 310–313.
- [19] H. Kaur, J. Kaur, L. Singh, S. Singh, *Superlattices Microstruct.* **2013**, *64*, 294–302.
- [20] L. Zhang, W. He, X. Chen, Y. Du, X. Zhang, Y. Shen, F. Yang, *Surf. Sci.* **2015**, *631*, 173–177.
- [21] H. Kim, S. Ballikaya, H. Chi, J.-P. Ahn, K. Ahn, C. Uher, M. Kaviani, *Acta Mater.* **2015**, *86*, 247–253.
- [22] F. Gao, S. L. Leng, Z. Zhu, X. J. Li, X. Hu, H. Z. Song, *J. Electron. Mater.* **2018**, *47*, 2454–2460.
- [23] X. T. Tran, S. Poorahong, M. Sij, *RSC Adv.* **2017**, *7*, 52345–52351.
- [24] X. Han, F. Liao, Y. Zhang, Z. Yuan, H. Chen, C. Xu, *Mater. Lett.* **2018**, *210*, 62–65.
- [25] K. Liu, H. Liu, J. Wang, L. Shi, *J. Alloys Compd.* **2009**, *484*, 674–676.
- [26] F. Jia, S. Zhang, X. Zhang, X. Peng, H. Zhang, Y. Xiang, *Chem. Eur. J.* **2014**, *20*, 15941–15946.
- [27] M. Schuster, M. Distaso, S. A. Möckel, U. Künecke, W. Peukert, P. J. Wellmann, *Energy Procedia* **2015**, *84*, 62–70.
- [28] H. E.-D. M. Saleh, M. Koller in *Green Chemistry*, Introductory chapter: principles of green chemistry, IntechOpen, **2018**, pp. 3–13.
- [29] F.-H. Lin, C.-J. Liu, *Green Chem.* **2016**, *18*, 5288–5294.
- [30] F.-H. Lin, C.-J. Liu, *Ceram. Int.* **2019**, *45*, 9397–9400.
- [31] G. N. Glavee, K. J. Klabunde, C. M. Sorensen, G. C. Hadjipanayis, *Langmuir* **1994**, *10*, 4726–4730.
- [32] D. L. Klayman, T. S. Griffin, *J. Am. Chem. Soc.* **1973**, *95*, 197–199.
- [33] S. Licht, F. Forouzan, *J. Electrochem. Soc.* **1995**, *142*, 1546–1551.
- [34] F. W. Bergstrom, *J. Am. Chem. Soc.* **1926**, *48*, 146–151.
- [35] S. C. Riha, D. C. Johnson, A. L. Prieto, *J. Am. Chem. Soc.* **2011**, *133*, 1383–1390.
- [36] A. F. May, G. J. Snyder, D. M. Rowe, in *Materials Preparation, and Characterization in Thermoelectrics*, CRC, Boca Raton, USA, **2012**, pp. 1–12.
- [37] E.-Y. Liu, H.-H. Lin, Z.-R. Yang, C.-J. Liu, *R. Soc. Open Sci.* **2018**, *5*, 180698.
- [38] C.-A. Wu, K.-C. Chang, F.-H. Lin, Z.-R. Yang, A. Gharleghi, T.-Z. Wei, C.-J. Liu, *Chem. Eng. J.* **2019**, *368*, 409–416.
- [39] K.-C. Chang, C.-J. Liu, *Comput. Phys. Commun.* **2020**, *247*, 106875.

Manuscript received: November 28, 2020
Revised manuscript received: December 21, 2020
Accepted manuscript online: January 5, 2021
Version of record online: January 28, 2021